Available online at www.sciencedirect.com
ScienceDirect
Journal of Solid State Chemistry 180 (2007) 3026–3034
JOURNAL OF SOLID STATE CHEMISTRY
www.elsevier.com/locate/jssc

Low-temperature single crystal X-ray diffraction and high-pressure Raman studies on $[(CH_3)_2NH_2]_2[SbCl_5]$

Maciej Bujak*, Ross J. Angel

Crystallography Laboratory, Department of Geosciences, Virginia Tech, Blacksburg, VA 24061, USA

Received 7 May 2007; received in revised form 24 August 2007; accepted 26 August 2007
Available online 6 September 2007

Abstract

The structure of bis(dimethylammonium) pentachloroantimonate(III), $[(CH_3)_2NH_2]_2[SbCl_5]$, BDP, was studied at 15 K and ambient pressure by single-crystal X-ray diffraction as well as at ambient temperature and high pressures up to 4.87(5) GPa by Raman spectroscopy. BDP crystallizes in the orthorhombic *Pnma* space group with $a = 8.4069(4)$, $b = 11.7973(7)$, $c = 14.8496(7)$ Å, and $Z = 4$; $R_1 = 0.0381$, w$R_2 = 0.0764$. The structure consists of distorted $[SbCl_6]^{3-}$ octahedra forming zig-zag $[\{SbCl_5\}_n]^{2n-}$ chains that are cross-linked by dimethylammonium $[(CH_3)_2NH_2]^+$ cations. The organic and inorganic substructures are bound together by the N–H…Cl hydrogen bonds. The distortions of $[SbCl_6]^{3-}$ units increase, partly due to the influence of the hydrogen bonds which became stronger, with decreasing temperature. The preliminary room temperature, high-pressure X-ray diffraction experiments suggest that BDP undergoes a first-order phase transition below ca. 0.44(5) GPa that destroys single-crystal samples. The transition is accompanied by changes in the intensities and positions of the Raman lines below 400 cm^{-1}.

Keywords: Chloroantimonates(III); Phase transition; Hydrogen bonding; Polyhedral distortions

1. Introduction

The halogenoantimonates(III) and halogenobismuthates(III) with organic cations have potential applications as "designer" ferroic materials because they display a broad range of ferroic transitions that can be tailored by choice of the inorganic framework and the organic cations. One of the most interesting subgroups, from the point of view of materials properties, are crystals of general formulae $R_5M_2X_{11}$ and $R_3M_2X_9$ (R—organic cations; M—Sb^{III}, Bi^{III}; X—Cl, Br, I) with relatively small alkylammonium cations, e.g. [1–3]. These materials exhibit electro-optic activity and transitions to ferroelastic and ferroelectric phases. Our research program is aimed at understanding the factors that determine the formation of the different anionic substructures and the distortions of inorganic polyhedra, and the forces that drive and control the ferroic phase transitions with the goal of predicting their properties and the phase transition behavior from their structures, e.g. [4–7]. In this context, comparison of the high-pressure structural evolution and phase transitions of a given compound with those observed with changing temperature provides the opportunity to separate dynamic from static effects.

The halogenoantimonates(III) and halogenobismuthates(III) with organic cations can be obtained by reacting an organic substance and antimony(III)/bismuth(III) salt (oxide) in the appropriate solvent. It is a general characteristic that, depending on the ratio of reactants, one or more products of the general formula $R_aM_bX_{a+3b}$ (a, b—stoichiometric coefficients) can be crystallized using the same starting materials, e.g. [5–8]. Dimethylammonium chloroatimonates(III) illustrate such behavior. On changing the molar ratio of dimethylamine to antimony(III) chloride from 0.1:1 to 10:1 three structurally different chloroantimonates(III), ferroic $[(CH_3)_2NH_2]_2[Sb_2Cl_9]$ (DMACA), $[(CH_3)_2NH_2]_2[SbCl_5]$ (BDP) and $[(CH_3)_2NH_2]_3[SbCl_6]\cdot[(CH_3)_2NH_2]Cl$ showing different properties, were obtained. For molar ratios between 0.6:1 and 5.5:1

*Corresponding author. Permanent address: Institute of Chemistry, University of Opole, Oleska 48, 45-052 Opole, Poland.
Fax: +48 77 452 7175.
E-mail address: mbujak@uni.opole.pl (M. Bujak).

0022-4596/$ - see front matter © 2007 Elsevier Inc. All rights reserved.
doi:10.1016/j.jssc.2007.08.025

DMACA crystals were obtained. Increasing the molar ratio of substrates to the 5.5:1–9.5:1 range leads to crystallization of BDP. Additional increase in the ratio to between 9.5:1 and 10:1 results in crystallization of $[(CH_3)_2NH_2]_3[SbCl_6]\cdot[(CH_3)_2NH_2]Cl$ [5]. The structures of all of these compounds are built of corner-sharing or isolated $[SbCl_6]^{3-}$ octahedra with dimethylammonium cations located in the cavities formed by the inorganic substructures [6,9–13]. In the structures of BDP and DMACA, in which inorganic octahedra share corners to form polymeric chains and layers, respectively, the $[SbCl_6]^{3-}$ units are significantly distorted. These distortions are associated with the presence of the $5s^2$ lone-electron pair located on the central Sb^{III} atom [14,15] and depend on two principal factors. The 'primary' deformation results from the polyhedra sharing halogen atoms with each other, along with secondary bonding effects within the framework so formed [16,17]. The 'secondary' deformation arises from the interactions of the framework with the oppositely charged organic cations, e.g. [18,19].

In our previous papers we have shown that these distortions, marked by significant differences in the Sb–Cl bond lengths and Cl(Sb)–Sb(Cl)–Cl(Sb) angles, increase with decreasing temperature or increasing pressure. Smaller changes are associated with either ordering of the organic cations or a decrease of the donor…acceptor distances of hydrogen bonds with decreasing temperature [6,12], but the largest changes occur across temperature- or pressure-induced phase transitions and with increasing pressure alone [7,11].

The phase transitions in the chloroantimonates(III), and in the whole family of halogenoantimonates(III) and halogenobismuthates(III), e.g. [20–22], are mainly related to the large polarizability of the complex inorganic anions, changes in the dynamic disorder of the organic cations and consequent changes in the hydrogen-bonding scheme [11,15]. In the absence of changes in the state of dynamic disorder of organic cations, the structural changes and phase transitions can also arise from intrinsic processes in the inorganic component of the structure alone [7]. Previous ambient-pressure investigations on the structure of BDP [12] showed considerable changes in the geometries of hydrogen-bonding between 295 and 85 K that result in significant distortions of $[SbCl_6]^{3-}$ octahedra. No phase transitions were found, perhaps because the dimethylammonium cations are already ordered at room temperature. By contrast, the similar R_2SbCl_5 chloroantimonate(III) $[(CH_3)_2NH(CH_2)_2NH_3][SbCl_5]$, NNDP [7], undergoes a pressure-induced phase transition which results in the formation of new Sb–Cl bonds at high pressures. We have therefore explored the low-temperature (down to 15 K) and high-pressure behavior of the BDP structure. Here we report our further observations on the role of the lone-electron pair and the hydrogen-bonding between chlorine ligands and organic cations on the distortions of the $[SbCl_6]^{3-}$ octahedral geometry, as well as the importance of the dynamic state of the organic cations and types of inorganic substructure on the phase transition behavior in this particular dimethylammonium chloroantimonate(III).

2. Experimental

2.1. Preparation of single crystals of BDP

Antimony(III) oxide (puriss. p.a., Fluka), dimethylamine (40 wt% solution in water, Acros Organics) and concentrated hydrochloric acid (36.5–38%, EM Science) were the starting materials used for the synthesis of BDP. 2.915 g (10 mmol) Sb_2O_3 dissolved in ca. 25 mL of hot concentrated HCl were treated with 22.8 mL (180 mmol) of dimethylamine dissolved in 30.0 mL of ca. 6 M HCl. The acid solution was allowed to slowly evaporate at room temperature until the transparent, colorless crystals were grown.

2.2. Low-temperature X-ray measurement and structure determination

Intensity data were collected on an Oxford Diffraction Xcalibur-2 diffractometer equipped with an Enhance X-ray source, a Sapphire-3 CCD detector and an Oxford Diffraction Helijet cooler. The reflections were measured using the φ- and ω-scan techniques with $\Delta\omega$ (or $\Delta\varphi$) $= 1.0^\circ$ and $\Delta t = 5$ s. The unit-cell parameters were obtained from a least-squares refinement to the positions of 10 520 reflections harvested from the resulting images. The data were subjected to Lorentz, polarization and numerical absorption corrections [23]. The Oxford Diffraction CrysAlis CCD and CrysAlis RED programs were used during the data collection, cell refinement and data reduction processes [23]. SHELXTL NT was used for the structure solution and refinement [24]. The structure was solved by the Patterson method. All hydrogen atoms were located in the subsequent maps, refined and constrained to the same distance (SADI command of SHELXTL NT) for $-CH_3$, $>NH_2^+$ groups. The displacement parameters of H-atoms were set at 1.5 and 1.2 times larger than the respective parameters of the methyl carbon and nitrogen atoms. The structure drawings were prepared using the XP program within SHELXTL NT [24]. The crystal data and the structure determination details for BDP at 15 K are listed in Table 1. The final atomic coordinates and equivalent isotropic displacement parameters for non-hydrogen atoms are shown in Table 2. The bond lengths, angles and the hydrogen-bonding geometries are presented in Tables 3 and 4. Crystallographic data (excluding structure factors) for bis(dimethylammonium) pentachloroantimonate(III), BDP, at 15 K have been deposited at the Cambridge Crystallographic Data Centre as supplementary publication no. CCDC 645987. Copies of the data can be obtained, free of charge, on application to the Director, CCDC, 12 Union Road, Cambridge CB2 1EZ, UK (Fax: (44) 1223 336-033; e-mail: deposit@ccdc.cam.ac.uk).

Table 1
The crystal data and structure determination summary for BDP

Temperature (K)	15
Pressure (MPa)	0.1
Empirical formula	$C_4H_{16}Cl_5N_2Sb$
Formula weight	391.19
Crystal color; habit	Colorless; tabular
Crystal size (mm^3)	$0.20 \times 0.18 \times 0.08$
Crystal system	Orthorhombic
Space group	*Pnma*
Unit cell dimensions (Å)	$a = 8.4069(4)$
	$b = 11.7973(7)$
	$c = 14.8496(7)$
Volume ($Å^3$)	1472.76(13)
Z	4
Density (calculated) ($g\,cm^{-3}$)	1.764
Wavelength (Å)	Mo$K\alpha$, $\lambda = 0.71073$
Absorption coefficient (mm^{-1})	2.745
$F(0\,0\,0)$	760
θ Range (deg.)	4.05–25.00
Index ranges	$-9 \leqslant h \leqslant 9$; $-14 \leqslant k \leqslant 14$; $-17 \leqslant l \leqslant 17$
Reflections collected/unique	18 994/1298 ($R_{int} = 0.0271$)
Observed reflections [$I > 2\sigma(I)$]	1225
Data/parameters	1298/85
Goodness of fit on F^2	1.180
Final R indices [$I > 2\sigma(I)$][a]	$R_1 = 0.0357$, w$R_2 = 0.0750$
R indices (all data)[a]	$R_1 = 0.0381$, w$R_2 = 0.0764$
Largest diff. peak/hole ($e\,Å^{-3}$)	1.598/−0.879

[a] $R_1 = \Sigma||F_o|-|F_c||/\Sigma|F_o|$; w$R_2 = \{\Sigma[w(F_o^2-F_c^2)^2]/\Sigma[w(F_o^2)^2]\}^{1/2}$.

Table 2
Atomic coordinates ($\times 10^4$) and equivalent isotropic displacement parameters ($Å^2 \times 10^3$) for non-hydrogen atoms of BDP at 15 K

Atom	x	y	z	U_{eq}[a]
Sb(1)	7972(1)	7500	5978(1)	11(1)
Cl(1)	8054(1)	9714(1)	5904(1)	13(1)
Cl(2)	10 098(2)	7500	4893(1)	14(1)
Cl(3)	5989(2)	7500	4744(1)	15(1)
Cl(4)	10634(2)	7500	7206(1)	15(1)
N(1)	8063(4)	10 218(3)	3768(2)	15(1)
C(1)	8370(5)	92 72(4)	3122(3)	18(1)
C(2)	6362(5)	10 558(4)	3830(3)	20(1)

[a] U_{eq} is defined as one third of the trace of the orthogonalized U_{ij} tensor.

2.3. High-pressure Raman measurements

Raman spectra were recorded with a Jobin Yvon Horiba Lab Ram HR800 spectrometric analyzer, integrated with a confocal microscope, in two spectral regions 50–1250 and 1430–3700 cm^{-1} (to avoid the strong Raman line from the diamond anvils at ca. 1332 cm^{-1}) using a water-cooled CCD multichannel detector. The Raman system provides a resolution of 0.3–1 cm^{-1}. The 514.57 nm line from an Ar-ion laser was used as an excitation source. The laser beam was passed through a vertical polarizer and a tunable filter and focused on to the sample using a microscope objective ($10\times$). The data were averaged over two collection periods of 10 s (5 s for the diamond-anvil cell alone and dimethylammonium hydrochloride) each for each spectrum. The single-crystal sample of BDP was loaded and pressurized in a Brillouin-Raman diamond-anvil cell (High Pressure Diamond Optics, Inc., Tuscon, AZ, USA) equipped with diamond anvils (culet diameter 0.62 mm) mounted on hardened steel seats. The gasket, made of 0.25 mm thick hard T301 steel foil, was pre-indented to a thickness of ca. 0.22 mm, and then a hole of 0.30 mm in diameter was spark-eroded in the center of the indented region. The sample crystal was placed on the surface of an anvil together with a small ruby ball (ca. 0.02 mm in diameter), without using any grease or glue. Cryogenically loaded nitrogen was used as pressure-transmitting medium. Previous measurements indicated that nitrogen remains hydrostatic up to its freezing pressure of 3.0 GPa at room temperature, and supports some deviatoric stresses at the maximum pressure of ca. 4.9 GPa achieved in these experiments [25]. Pressures, during both high-pressure Raman and preliminary X-ray experiments, were determined from the shift of the ruby R-luminescence lines [26] using the same Lab Ram HR800 instrument. The precision in our pressure measurements was estimated to be ~0.05 GPa.

3. Results and discussion

3.1. Phase I—structure of BDP at 15 K and ambient pressure

At 15 K and ambient pressure the structure of BDP retains the same *Pnma* space group as well as anionic and cationic substructures as previously reported at 295 and 85 K [12]. We designate this structure as phase I. There is half an Sb atom, two and a half Cl atoms and one dimethylammonium cation in the asymmetric unit. The antimony atom and three chlorine ligands (one bridging Cl(4) and two terminal Cl(2), Cl(3)) are located on special positions (Table 2).

The inorganic substructure of BDP is built from $[SbCl_6]^{3-}$ octahedra connected by *cis*-corners to form zig-zag polymeric $[\{SbCl_5\}_n]^{2n-}$ chains extended along the *a*-axis (Fig. 1). In the coordination sphere of Sb(1) two chlorine atoms, Cl(4) and Cl(4)^{II} are bridging and four, Cl(1), Cl(1)^{I}, Cl(2) and Cl(3), are terminal. At 15 K the $[SbCl_6]^{3-}$ octahedron is significantly distorted, with Sb–Cl distances ranging from 2.4065(14) to 3.3370(14) Å (Table 3, Fig. 2). The shortening of the terminal Sb(1)–Cl(2) and Sb(1)–Cl(3) bonds appears to be an example of *trans*-influence [19,27], that is a response to the lengthening of bridging Sb(1)–Cl(4) and Sb(1)–Cl(4)^{II} distances. The angles involving Cl atoms mutually *cis* range from 81.22(4)° to 101.60(4)°, while the *trans* angles are 168.13(4)°, 171.49(4)°, and 174.32(4)°. This coordination is similar to that found in other chloroantimonate(III) crystals in which anionic substructures are also built of polymeric $[\{SbCl_5\}_n]^{2n-}$ chains, e.g. [22,28,29].

Table 3
Selected bond lengths (Å), angles (deg.) and their differences for BDP at 15, 85 and 295 K [12] and ambient pressure

Atoms/temperature (K)	15	85	295	Δ(295–15)	Δ(85–15)
Sb(1)–Cl(1)/Cl(1)^{I}	2.6157(10)	2.615(1)	2.616(1)	0.000	−0.001
Sb(1)–Cl(2)	2.4065(14)	2.405(1)	2.404(1)	−0.002	−0.002
Sb(1)–Cl(3)	2.4770(14)	2.474(1)	2.475(1)	−0.002	−0.003
Sb(1)–Cl(4)	2.8865(14)	2.900(1)	2.873(1)	−0.013	0.014
Sb(1)–Cl(4)^{II}	3.3370(14)	3.306(1)	3.257(1)	−0.080	−0.031
N(1)–C(1)	1.494(5)	1.480(5)	1.481(7)	−0.013	−0.014
N(1)–C(2)	1.488(5)	1.478(5)	1.443(7)	−0.045	−0.010
Cl(1)–Sb(1)–Cl(1)^{I}	174.32(4)	174.01(4)	173.99(4)	−0.33	−0.31
Cl(1)/Cl(1)^{I}–Sb(1)–Cl(2)	87.27(2)	87.17(2)	87.20(2)	−0.07	−0.10
Cl(1)/Cl(1)^{I}–Sb(1)–Cl(3)	89.22(2)	89.03(2)	88.90(2)	−0.32	−0.19
Cl(1)/Cl(1)^{I}–Sb(1)–Cl(4)	90.36(2)	90.56(2)	90.71(2)	0.35	0.20
Cl(1)/Cl(1)^{I}–Sb(1)–Cl(4)^{II}	92.83(2)	92.96(2)	92.92(2)	0.09	0.13
Cl(2)–Sb(1)–Cl(3)	90.27(5)	90.30(4)	89.87(5)	−0.40	0.03
Cl(2)–Sb(1)–Cl(4)	81.22(4)	81.52(4)	82.37(4)	1.15	0.30
Cl(2)–Sb(1)–Cl(4)^{II}	168.13(4)	170.13(4)	172.75(4)	4.62	2.00
Cl(3)–Sb(1)–Cl(4)	171.49(4)	171.83(4)	172.24(4)	0.75	0.34
Cl(3)–Sb(1)–Cl(4)^{II}	101.60(4)	99.56(4)	97.38(4)	−4.22	−2.04
Cl(4)–Sb(1)–Cl(4)^{II}	86.915(12)	88.61(2)	90.38(2)	3.46	1.69
Sb(1)–Cl(4)–Sb(1)^{III}	165.27(5)	166.46(4)	168.44(4)	3.17	1.19
C(1)–N(1)–C(2)	114.0(3)	114.1(4)	115.5(5)	1.5	0.1

Symmetry codes: (I) x, $-y+3/2$, z; (II) $x-1/2$, y, $-z+3/2$; (III) $x+1/2$, y, $-z+3/2$.

Table 4
The N–H…Cl hydrogen bond geometries (Å, deg.) at 15, 85 and 295 K [12] and ambient pressure for BDP

D–H…A	D–H	H…A	D…A	D–H…A
15 K				
N(1)–H(1E)…Cl(1)	0.87(3)	2.46(4)	3.227(4)	147(4)
N(1)–H(1D)…Cl(4)^{I}	0.87(3)	2.40(4)	3.247(4)	165(4)
85 K				
N(1)–H(1E)…Cl(1)	0.83(3)	2.45(4)	3.236(3)	159(4)
N(1)–H(1D)…Cl(4)^{I}	0.85(3)	2.48(4)	3.275(3)	157(4)
295 K				
N(1)–H(1E)…Cl(1)	0.88(5)	2.46(6)	3.266(4)	153(6)
N(1)–H(1D)…Cl(4)^{I}	0.90(6)	2.63(6)	3.353(4)	138(6)

Symmetry code: (I) $-x+2$, $-y+2$, $-z+1$.

The organic substructure of BDP consists of ordered dimethylammonium $[(CH_3)_2NH_2]^+$ cations located between the inorganic chains (Fig. 1). The bond distances and valence angles of the cations (Table 3) are typical of those observed in other compounds containing dimethylammonium cations [6,12,30].

The dimethylammonium cations are linked to the inorganic $[\{SbCl_5\}_n]^{2n-}$ chains through the N–H…Cl hydrogen bonds, and are thus partly responsible for the distorted octahedral coordination of the Sb^{III}, both in terms of differences between equivalent Sb–Cl distances and Cl(Sb)–Sb(Cl)–Cl(Sb) angles. The influence of these intermolecular interactions is clearly seen in the geometrical parameters involving the weakest-bonded bridging chlorine atoms (Fig. 2). The presence of relatively strong hydrogen bonds partly causes significant distortion of the inter-octahedral Sb(1)–Cl(4)–Sb(1)^{III} angle (165.27(5)°) from its ideal value of 180°. The comparison of the observed Sb–Cl bond lengths with the geometry of the isolated $[SbCl_6]^{3-}$ octahedron found in the structure of $[Co(NH_3)_6][SbCl_6]$ [31] further confirms that the distortions of the octahedra mainly result from the interactions between $[SbCl_6]^{3-}$ units and, in addition, are affected by the interactions between oppositely charged organic and inorganic components of the structure. Thus, while the Sb–Cl bond lengths of the isolated $[SbCl_6]^{3-}$ octahedron in $[Co(NH_3)_6][SbCl_6]$ are 2.643(6) Å (2.652(6) Å when corrected assuming a riding model), the average Sb–Cl bond length in BDP at 15 K for two terminal *trans* ligands is 2.6157 Å, for two terminal Cl atoms located *trans* to bridging ones it is 2.4418 Å, and for two bridging Sb–Cl distances it is 3.1118 Å (Table 3).

3.2. Phase I—evolution with temperature

The a and b unit-cell parameters of BDP decrease almost linearly, whereas the c parameter slightly increases with decreasing temperature from 295 to 15 K. The lengths of the a and b unit-cell parameters decrease by 2.23% and 1.62%, whereas the c parameter increases by 0.04%. As a result, the unit-cell volume at 15 K is 3.79% less than at room temperature (Table 1) [12].

Temperature has little effect upon the bond lengths and angles of the organic part of the structure, but significant changes were found for the inorganic substructure, particularly the geometrical parameters involving the bridging Cl(4)^{II} atom and its N–H…Cl interactions (Table 4).

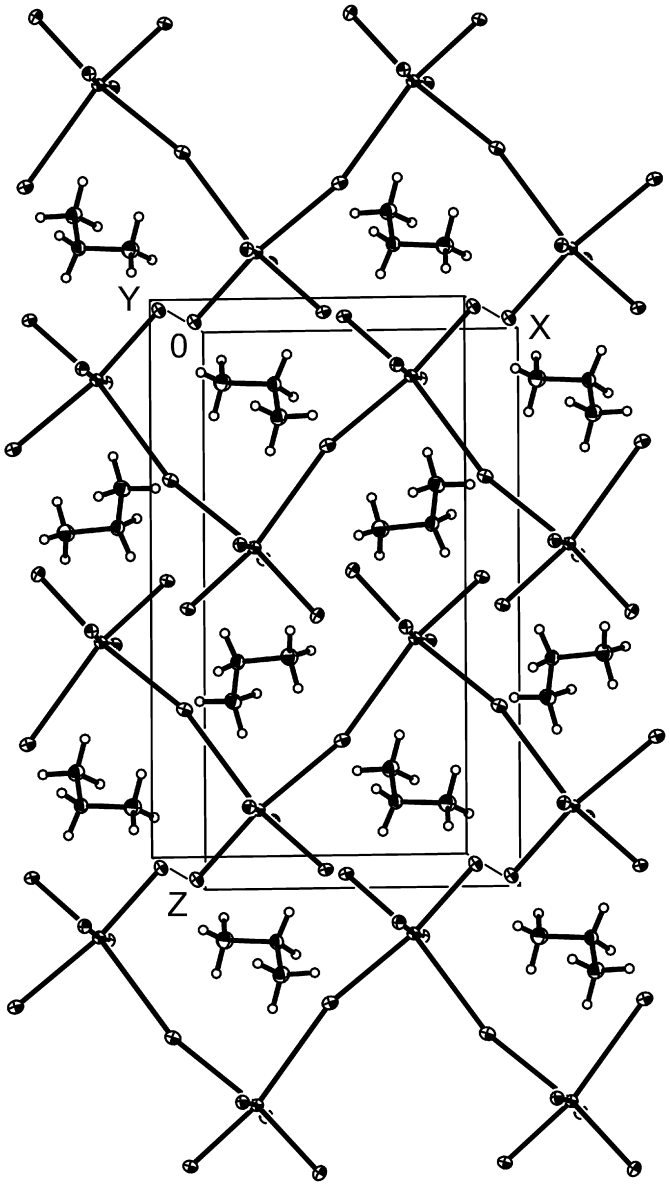

Fig. 1. The structure of BDP at 15 K and ambient pressure. Displacement ellipsoids are plotted at the 50% probability level.

On cooling to 15 K, the Sb(1)–Cl(4)^{II} distance is elongated by 0.080 Å, the Cl(2)–Sb(1)–Cl(4)^{II}, Cl(4)–Sb(1)–Cl(4)^{II} and Sb(1)–Cl(4)–Sb(1)^{III} angles increase on average by 3.90°, whereas the Cl(3)–Sb(1)–Cl(4)^{II} angle decreases by 4.22° (Table 3). At the same time there are significant changes in the strength of N(1)–H(1D)…Cl(4)^{I} hydrogen bond—the N…Cl distance decreases by 0.106 Å, whereas the N–H…Cl angle increases by 27° (Table 4). The significant decrease of the inter-octahedral Sb(1)–Cl(4)–Sb(1)^{III} angle (parallel to [100]) together with increasing of the strength of N–H…Cl hydrogen bond seems to be responsible for the [100] direction (direction of extension of the $[\{SbCl_5\}_n]^{2n-}$ chains) having the greatest thermal expansion coefficient. A similar situation was observed for NNDP in which both the highest thermal expansion and compressibility is along the direction of the chains of the $[SbCl_5]^{2-}$ square pyramids [7]. It should be emphasized that, besides the N(1)–H(1D)…Cl(4)^{I}, the second N(1)–H(1E)…Cl(1) hydrogen bond also changes with decreasing temperature (Table 4). But in this case the changes in the geometry of the hydrogen bond alone are not so significant and therefore the influence of these interactions on the terminal and relatively short Sb(1)–Cl(1)/Cl(1)^{I} distances is within the experimental uncertainties (Table 3).

The significant influence of the hydrogen bonds on the bridging chlorine ligands and, consequently, the distortions of the BDP octahedral $[SbCl_6]^{3-}$ units is further confirmed by the analysis of the changes in the bond-length distortion parameter $\Delta = \frac{1}{6}\sum_{i=1}^{6}[(R_i - \overline{R})/\overline{R}]^2$ calculated from $\overline{R}$, the average Sb–Cl bond length within the octahedron, and R_i, the individual Sb–Cl bond lengths [32,33]. Both Sb and Cl atoms occupy the same general or special positions in the structure of phase I at temperatures between 295 and 15 K, so their coordination geometry is not related to phase transitions or symmetry changes. In the structures of TMACA [5,6,34], DMACA [6,11] and NNDP [7,35] the hydrogen bonds become, in general, stronger with decreasing temperature, and the inorganic octahedra become less distorted. But the opposite occurs in BDP; while the hydrogen bonds also become stronger with decreasing temperature, the $\Delta \times 10^3$ parameters significantly increase from 11.63 at 295 K to 13.20 at 15 K. This is supported by the observation that the deviation from the Sb–Cl bond lengths from the 2.643(6) Å (2.652(6) Å) of the reference octahedron in $[Co(NH_3)_6][SbCl_6]$ [31] is larger at 15 K than at room temperature.

3.3. Phase II—high pressure

On the basis of previous studies we know that cooling this class of compounds to 15 K at ambient pressure results in structural changes that are similar to those obtained by applying a pressure of ca. 0.4–0.5 GPa at room temperature [7,36,37]. Thus higher pressures result in novel behavior not observed at low temperatures. We loaded a single crystal of BDP in to an ETH diamond-anvil cell [38] using the same procedures as for NNDP [7] and cryogenically loaded nitrogen as the pressure medium. We found that the single crystals of BDP were always destroyed at pressures of ~0.5 GPa (Fig. 3), marked by the appearance of cracks in the crystal. Examination of recovered samples confirmed that they were significantly thinner than the gasket in the diamond-anvil cell. We also know that nitrogen remains hydrostatic in this pressure regime [25]. Therefore, the mechanical destruction of the crystals is not the result of non-hydrostatic stresses but arises from the application of hydrostatic pressure alone. We were unable to satisfactory index the resulting diffraction patterns collected with a CCD detector, and there is no indication from these diffraction patterns that the room-pressure phase remains. We therefore conclude that a first-order phase transition

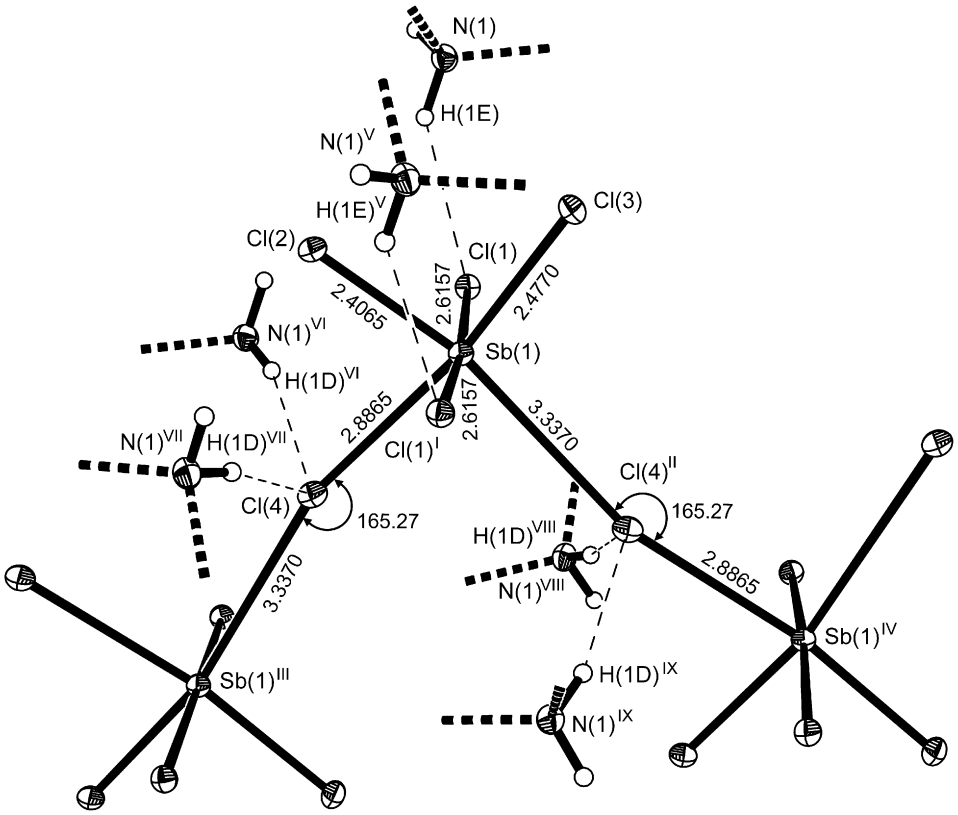

Fig. 2. The N–H…Cl hydrogen bonds (thin dashed lines) involving Cl(1), $Cl(1)^{I}$, Cl(4) and $Cl(4)^{II}$ atoms that partly contribute to the deformation of the $[SbCl_6]^{3-}$ octahedron in the structure of BDP at 15 K and ambient pressure. Displacement ellipsoids are plotted at the 50% probability level. Symmetry codes: (I) $x, -y+3/2, z$; (II) $x-1/2, y, -z+3/2$; (III) $x+1/2, y, -z+3/2$; (IV) $x-1/2, y, -z+3/2$; (V) $x, y-1/2, z$; (VI) $-x+2, -y+2, -z+1$; (VII) $-x+2, y-1/2, -z+1$; (VIII) $-x+3/2, -y+2, z+1/2$; (IX) $-x+3/2, y-1/2, z+1/2$.

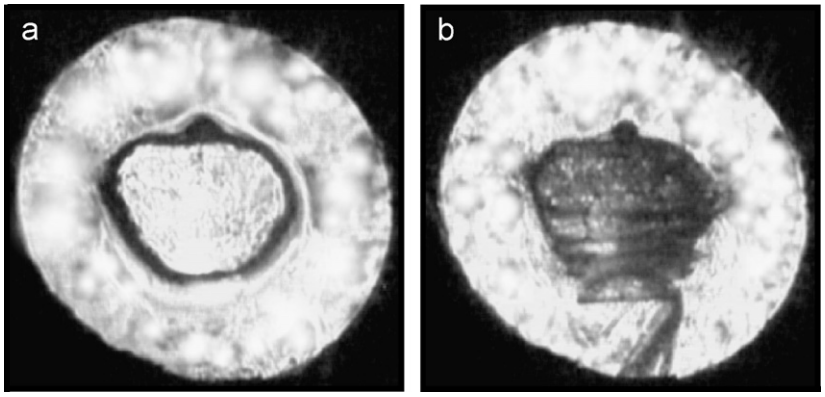

Fig. 3. The crystal sample of BDP in the high-pressure diamond-anvil cell at: (a) ambient pressure, 0.1 MPa and (b) 0.44(5) GPa, during the preliminary X-ray diffraction experiment. Cryogenically loaded nitrogen was used as a pressure-transmitting medium [25]. A small ruby ball, used as a pressure marker, is visible near the top edge of the crystal. The mottled appearance outside the crystal is, in part, due to petroleum jelly used for fixing the sample and ruby ball on one of the diamond anvils.

occurs between room pressure and 0.5 GPa to a new structure which we designate as phase II.

Raman spectroscopy does not require large single crystals, and was therefore used to try and confirm the presence of a phase transition. Fig. 4 presents the Raman spectra of the BDP sample collected at selected high-pressure points and, for comparison, the ambient-condition spectra of the diamond-anvil cell alone and dimethylammonium hydrochloride. The Raman spectra of BDP show strong bands, which are assignable to the inorganic and organic components of the structure because their vibrational frequencies are known from other compounds [29,39,40].

The strong lines in the low-frequency range, below 400 cm^{-1} are similar to those in analogous structures [9] and those containing bismuth instead of antimony [41,42].

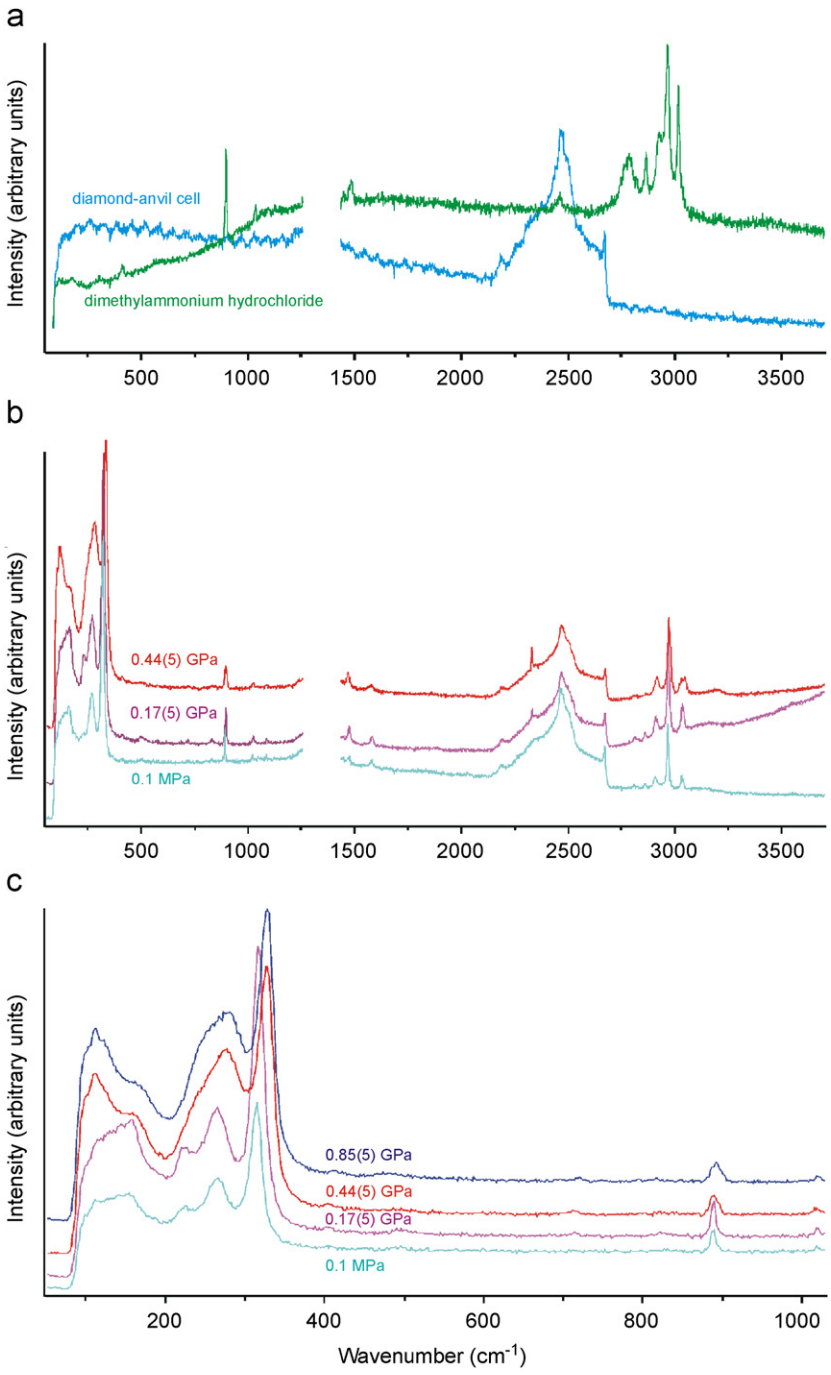

Fig. 4. (a) The superimposed room-temperature Raman spectra of the diamond-anvil cell alone and dimethylammonium hydrochloride at ambient pressure, 0.1 MPa. (b) Spectra of the BDP sample at 0.1 MPa, 0.17(5) and 0.44(5) GPa. (c) Spectra of the BDP sample at 0.1 MPa, 0.17(5), 0.44(5), and 0.85(5) GPa.

They are associated with the Sb–Cl stretching modes for the terminal (ca. 315 cm^{-1}), bridging Sb–Cl bonds (ca. 260 and 215 cm^{-1}) and the Cl–Sb–Cl bending vibrations (ca. 150 cm^{-1}). At 0.17(5) GPa the Raman spectrum is very similar to that obtained at ambient conditions, and is thus consistent with BDP remaining in phase I. By contrast, there are significant differences in positions, line widths and shapes of these Raman lines in the spectra collected at 0.44(5) GPa. The stretching vibrations of both terminal and bridging Sb–Cl are shifted to higher frequencies and their intensities change. Marked changes of the Cl–Sb–Cl bending vibrations are also observed, and with increasing pressure the widths of these low-frequency lines increase. In the high-frequency regime the spectra are essentially unchanged. Therefore, the spectra are indicative of stronger interactions among the vibrational groups as pressure is increased to 0.44(5) GPa, but that strongly bonded $[\{SbCl_5\}_n]^{2n-}$ groups are preserved.

Further pressure increase from 0.44(5) to 4.87(5) GPa results in only very minor changes to the spectra, which suggests that BDP does not undergo any further phase transition, at least any that change the anionic substructure. Raman spectra of the samples after pressure release are identical to those of the starting material and indicate that the pressure-induced phase transition between phases I and II of BDP is reversible.

The low-temperature behavior of BDP together with the high-pressure transition behavior of NNDP [7] may provide some clues as to the nature of the high-pressure phase transition in BDP. The study of NNDP showed that pressures of ~0.5 GPa (at room temperature) resulted in structural changes greater than those induced by cooling to 15 K. Further, that study indicated that in $[\{SbCl_5\}_n]^{2n-}$ chains of $[SbCl_6]^{3-}$ octahedra, Sb–Cl bridging distances of ~3.4 Å are unstable; in NNDP when the bonds are compressed to this value a phase transition occurs and produces alternating Sb–Cl bridging distances of ca. 3.30 and 3.56 Å. In BDP we have seen that decreasing temperature leads to significant shortening of the N(1)–H(1D)…Cl(4)^{I} hydrogen bond (Table 4), which at 15 K can be considered to be one of the strongest in chloroantimonates(III). This shortening contributes to an elongation of the Sb(1)–Cl(4)^{II} bond to 3.3370(14) Å, one of the longest bridging Sb–Cl bonds in chloroantimonates(III). Therefore, we suggest that the application of pressure to BDP might further shorten the N(1)–H(1D)…Cl(4)^{I} hydrogen bond, thereby lengthening the Sb(1)–Cl(4)^{II} distance into the unstable regime defined by the data for NNDP. The consequent breaking of at least some of these bonds in the $[\{SbCl_5\}_n]^{2n-}$ chains in BDP would then be responsible for the phase transition and destruction of the single crystal samples.

4. Summary and concluding remarks

This study of $[(CH_3)_2NH_2]_2[SbCl_5]$, BDP, provides a demonstration that the relative effects of quite modest pressures on the crystal structures of organic–inorganic hybrids far exceed the structural and physicochemical changes that occur on cooling even to helium temperatures. On cooling to 15 K, BDP exhibits significant changes in the detailed geometries of the longest Sb–Cl bonds that are correlated with the changes in the geometry of the hydrogen bonding. These changes are accomplished without any phase change, whereas even relatively low pressures induce a phase transition that is destructive for single crystals.

Further, these observations on BDP show that structural changes and phase transitions in organic–inorganic chloroantimonate(III) materials can be driven by changes occurring within inorganic components of the structure alone without the necessity of changes in the dynamic state of the organic cations. However, even without changes in their order, the organic cations do play an important role in determining the deformation of the inorganic framework. Clearly, in the structure of BDP the hydrogen bonds get stronger with decreasing temperature, and at the same time the Sb–Cl bridging bonds are significantly elongated. This shows that the so-called 'primary' and 'secondary' deformations of these structures should not be separated, but represent the direct influence of the hydrogen bonds on the distortions of inorganic substructures of chloroantimonates(III).

Acknowledgments

This material is based upon work supported by the North Atlantic Treaty Organization under a grant-fellowship awarded in 2004 (DGE-0410297). We acknowledge financial support from the National Science Foundation (CHE-0131128) for the purchase of the Oxford Diffraction Xcalibur-2 diffractometer. The Raman and ruby pressure measurements were conducted with the Raman system in the Vibrational Spectroscopy Laboratory in the Department of Geosciences at Virginia Tech. We are grateful to Drs. J. Zhao (Department of Geosciences), C. Slebodnick (Department of Chemistry), N. Vogelaar (Department of Biological Sciences, Virginia Tech) and Mr. D. Warner (Oxford Diffraction Ltd.) for valuable discussions and help during the experiments. We also thank Prof. B. Hanson (Department of Chemistry, Virginia Tech) for providing the starting materials and opportunity to prepare crystals in his laboratory.

References

[1] L. Sobczyk, R. Jakubas, J. Zaleski, Polish J. Chem. 71 (1997) 265–300.
[2] G. Bator, J. Baran, R. Jakubas, L. Sobczyk, J. Mol. Struct. 450 (1998) 89–100.
[3] R. Jakubas, G. Bator, Z. Ciunik, Ferroelectrics 295 (2003) 3–8.
[4] M. Bujak, L. Sikorska, J. Zaleski, Z. Anorg. Allg. Chem. 626 (2000) 2535–2542.
[5] M. Bujak, J. Zaleski, J. Solid State Chem. 177 (2004) 3202–3211.
[6] M. Bujak, R.J. Angel, J. Solid State Chem. 178 (2005) 2237–2246.
[7] M. Bujak, R.J. Angel, J. Phys. Chem. B 110 (2006) 10322–10331.
[8] U. Ensinger, W. Schwartz, A. Schmidt, Z. Naturforsch. 37b (1982) 1584–1589.
[9] F.J. Kruger, F. Zettler, A. Schmidt, Z. Anorg. Allg. Chem. 449 (1979) 135–144.
[10] M. Gdaniec, Z. Kostrukiewicz, R. Jakubas, L. Sobczyk, Ferroelectrics 77 (1988) 31–37.
[11] J. Zaleski, A. Pietraszko, Acta Cryst. B 52 (1996) 287–295.
[12] M. Bujak, J. Zaleski, Acta Cryst. C 54 (1998) 1773–1777.
[13] F. Knödler, U. Ensinger, W. Schwartz, A. Schmidt, Z. Anorg. Allg. Chem. 557 (1988) 208–218.
[14] R.J. Gillespie, E.A. Robinson, Chem. Soc. Rev. 34 (2005) 396–407.
[15] K.-Y. Akiba (Ed.), Chemistry of Hypervalent Compounds, Wiley-VCH Inc., New York, 1999.
[16] N.W. Alcock, Adv. Inorg. Radiochem. 15 (1972) 1–58.
[17] G.A. Landrum, R. Hoffmann, Angew. Chem. Int. Ed. 37 (1998) 1887–1890.
[18] M. Bujak, P. Osadczuk, J. Zaleski, Acta Cryst. C 57 (2001) 388–391.
[19] M. Bujak, J. Zaleski, Z. Naturforsch. 57b (2002) 157–164.
[20] R. Jakubas, Solid State Commun. 60 (1986) 389–391.
[21] R. Jakubas, Z. Czapla, Z. Galewski, L. Sobczyk, Ferroelectrics Lett. 5 (1986) 143–148.

[22] R. Jakubas, Z. Ciunik, G. Bator, Phys. Rev. B 67 (2003) 024103.
[23] Oxford Diffraction; CrysAlis CCD, Data collection GUI for CCD and CrysAlis RED CCD data reduction GUI, versions 1.171.24 beta (release 23.09.2004), Poland, 2004.
[24] G.M. Sheldrick, SHELXTL NT, 6.12, Bruker Analytical X-ray Systems Inc., Madison, WI, USA, 2001.
[25] R.J. Angel, M. Bujak, J. Zhao, G.D. Gatta, S.D. Jacobsen, J. Appl. Cryst. 40 (2007) 26–32.
[26] G.J. Piermarini, S. Block, J.D. Barnett, R.A. Forman, J. Appl. Phys. 46 (1975) 2774–2780.
[27] K.M. Anderson, A.G. Orpen, Chem. Commun. (2001) 2682–2683.
[28] M. Bujak, J. Zaleski, Main Group Met. Chem. 25 (2002) 583–584.
[29] U. Ensinger, W. Schwartz, A. Schmidt, Z. Naturforsch. 38b (1983) 149–154.
[30] N.A. Bokach, T.B. Pakhomova, V.Yu. Kukushkin, M. Haukka, A.J.L. Pombeiro, Inorg. Chem. 42 (2003) 7560–7568.
[31] D.R. Schroeder, R.A. Jacobson, Inorg. Chem. 12 (1973) 210–213.
[32] I.D. Brown, R.D. Shannon, Acta Cryst. A 29 (1973) 266–282.
[33] K. Robinson, G.V. Gibbs, P.H. Ribbe, Science 172 (1971) 567–570.
[34] M. Bujak, J. Zaleski, Cryst. Eng. 4 (2001) 241–252.
[35] M. Bujak, J. Zaleski, Z. Naturforsch. 56b (2001) 521–525.
[36] P. Guionneau, J. Gaultier, D. Chasseau, G. Bravic, Y. Barrans, L. Ducasse, D. Kanazawa, P. Day, M. Kurmoo, J. Phys. France 6 (1996) 1581–1595.
[37] P. Guionneau, C. Brigouleix, Y. Barrans, A.E. Goeta, J.F. Létard, J.A.K. Howard, J. Gaultier, D. Chasseau, Acad. Sci. Paris, Chemie/Chem. 4 (2001) 161–171.
[38] D.R. Allan, R. Miletich, R.J. Angel, Rev. Sci. Instrum. 67 (1996) 840–844.
[39] Th. Zeegers-Huyskens, G. Bator, Vibr. Spectrosc. 13 (1996) 41–49.
[40] G. Bator, R. Jakubas, J. Lefebvre, Y. Guinet, Vibr. Spectrosc. 18 (1998) 203–210.
[41] J. Laane, P.W. Jagodzinski, Inorg. Chem. 19 (1980) 44–49.
[42] B. Bednarska-Bolek, J. Zaleski, G. Bator, R. Jakubas, J. Phys. Chem. Solids 61 (2000) 1249–1261.